

# NUMERICAL SIMULATIONS OF CONSTRAINT AND SIZE EFFECTS IN FATIGUE CRACK GROWTH

Bo Wang and Thomas Siegmund

School of Mechanical Engineering, Purdue University, West Lafayette, IN, 47907

## ABSTRACT

The present paper describes results on investigations on fatigue crack growth (FCG) conducted by the use of an irreversible cohesive zone model. In the first part, the effects of constraint on FCG are investigated. Increased constraint leads to a reduction in crack closure and to an increase in crack growth rates. In the second part, the effect of size on FCG is investigated. For small structural dimensions damage is distributed homogeneously along the ligament in front of the crack tip, while as for large specimens damage is concentrated at the crack tip. Failure of small specimens is initiation dominated, while failure of large specimens is dominated by crack growth.

## 1 INTRODUCTION

Multi-layer structures are part of integrated circuitry and micro-electromechanical systems [1-4], and are also found in biological systems [5,6]. As structural length scales and associated layer thickness values decrease, two issues affect the fatigue failure behavior: constraint and size. As the thickness of individual layers is decreased in the multi-layer structure, the monotonic and cyclic plastic zones present at a crack tip can interact with the surrounding elastic material, leading to distortion of the plastic zone ahead of the crack tip [7-12]. Also, as the structural size decreases, the stress distribution at the crack tip changes [13]. Then, fatigue crack growth (FCG) analysis methodologies based on the Paris equation lose their validity and the transferability of FCG data among specimens with the different levels of constraint and of varying size is lost. To provide for an understanding of the constraint and size effects, and to enable the design of multi-layer structures at small scales against fatigue failure, an irreversible cohesive zone model (CZM) [14] is applied.

## 2 FORMULATION

An irreversible CZM is used to characterize the material separation under cyclic loading. This model describes the processes of material separation under cyclic loading by a constitutive relationship between the cyclically varying tractions and displacement jumps across an interface. Under monotonic loading the relationship between normal traction and normal separation,  $T_n$  and  $\Delta_n$ , is described by:

$$T_n = \sigma_{\max,0} e^{\left(\frac{\Delta_n}{\delta_0}\right)} \exp\left(-\frac{\Delta_n}{\delta_0}\right) \quad (1)$$

The CZ material parameters in (1) are the initial cohesive strength,  $\sigma_{\max,0}$ , and the cohesive length,  $\delta_0$ , such that the cohesive energy under monotonic loading is  $\phi_0 = \sigma_{\max,0} \delta_0 e$ . The irreversible CZM accounts for the evolution of the cohesive properties during cycling by use of a cyclic damage variable  $D_c$ . The constitutive relation for the CZM accounting for  $D_c$  is given by replacing the CZ tractions by the effective cohesive tractions. The initial cohesive strength,  $\sigma_{\max,0}$ , in (1) is substituted by the current cohesive strength,  $\sigma_{\max}$ , defined as

$$\sigma_{\max} = \sigma_{\max,0} (1 - D_c) \quad (2)$$

To obtain the current state of damage, an evolution equation for damage is provided:

$$\dot{D}_c = \frac{|\dot{\Delta}_n|}{\delta_\Sigma} \left[ \frac{T_n}{\sigma_{\max}} - \frac{\sigma_f}{\sigma_{\max,0}} \right] H(\bar{\Delta}_n - \delta_0) \quad \text{and} \quad \dot{D}_c \geq 0, \quad \bar{\Delta}_n = \int_t |\dot{\Delta}_n| dt \quad (3)$$

with  $H$  designating the Heaviside function. The CZ material parameters characterizing the fatigue behavior are the CZ endurance limit,  $\sigma_f$ , and,  $\delta_\Sigma$ , the accumulated cohesive length. Unloading and reloading are assumed to occur with the stiffness of  $T_{n,\max} / \Delta_{n,\max}$  such that during unloading/reloading the normal tractions are given by:

$$T_n = T_{n,\max} + T_{n,\max} / \Delta_{n,\max} (\Delta_n - \Delta_{n,\max}) \quad (4)$$

where  $T_{n,\max}$  is the normal traction corresponding to  $\Delta_{n,\max}$ , the maximum value of normal separation.

The irreversible CZM was implemented for the commercial finite element code ABAQUS by use of the UEL subroutine feature. The damage variable was defined on averaged variables per element [14].

### 3 CONSTRAINT EFFECTS

#### 3.1 Model Definition

A thin metal layer of height  $2h_l$  joins two elastic substrates with identical elastic properties. The crack is assumed to propagate along the center of the metal layer. The geometry of the problem addressed in this paper is shown in Fig. 1. In the modified boundary layer approach [15,16] loading is provided by describing boundary displacements according to prescribed cyclically varying mode I stress intensity factor  $K_I(t) = \Delta K(0.5 - 0.5 \cos 2\pi t)$ . Based on the mode I asymptotic crack tip solutions for linear elastic materials, the displacement fields are applied:

$$u_x(t) = K_I(t) \sqrt{\frac{r}{2\pi}} \frac{1+\nu}{E} \cos \frac{\theta}{2} (3 - 4\nu - \cos \theta) \quad u_y(t) = K_I(t) \sqrt{\frac{r}{2\pi}} \frac{1+\nu}{E} \sin \frac{\theta}{2} (3 - 4\nu - \cos \theta) \quad (5)$$

where  $r$  and  $\theta$  are polar coordinates of points on the remote outer boundary. We relate the range of the stress intensity factor,  $\Delta K$ , to the range of the energy release rate,  $\Delta G$ , by standard equations. Due to the nature of symmetry only half of the model is considered. The initial crack tip is located in a highly refined mesh region with length  $L$ . The length of one square element in this uniformly meshed region is  $l = 2.5\delta_0$ . The computations were carried out for a model with overall size  $r = 10000l$  and  $L = 110l$ . Four nodes plain strain elements are used. A single row of CZ elements was placed along the symmetry line of the model from the initial crack tip to the outer boundary. The CZ elements possess four nodes with linear displacement jump interpolation.

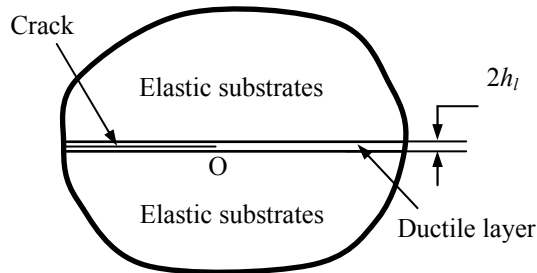


Figure 1: Schematic of a specimen where a ductile layer bonds two elastic substrates.

These elements use nodes on the line of symmetry as two of their nodes. The second pair of nodes of the CZ elements is those in common with the adjacent solid elements. The typical finite mesh consists of 3892 solid elements and 123 CZ elements. The metal layer and the adjoining elastic substrates possess identical isotropic elastic properties,  $E_s = E_l = 100$  GPa and  $\nu_s = \nu_l = 0.34$ . The elastic-plastic layer is characterized by a linear kinematic hardening model with yield strength  $\sigma_y = E_l/400$  and a hardening modulus of  $E_T = E_l/20$  [17], respectively. The values for the CZ parameters used in the computations are  $\phi_0 = 20$  J/m<sup>2</sup> and  $\sigma_{\max,0} = 4\sigma_y = E_l/100$  such that  $\delta_0 = 7.4$  nm. Furthermore, we assume  $\sigma_f / \sigma_{\max,0} = 0.25$  and  $\delta_\Sigma / \delta_0 = 4$ .

### 3.2 Results

The first set of results described was obtained under constant amplitude loading with  $\Delta G / \phi_0 = 0.25$  and a load ratio  $R=0$ . Figure 2(a) depicts the predicted increase in steady state FCG rate over that predicted for a model without constraint ( $h_l / \delta_0 \rightarrow \infty$ ),  $\{[d(\Delta a / \delta_0) / dN]_{h_l / \delta_0} - [d(\Delta a / \delta_0) / dN]_{h_l / \delta_0 \rightarrow \infty}\} / [d(\Delta a / \delta_0) / dN]_{h_l / \delta_0 \rightarrow \infty}$ , in dependence of the height of elastic-plastic layer. For the material parameters and the loading considered, a metal layer of height  $h_l / \delta_0 > 120$  is needed such that constraint effects vanish and the predicted FCG rate equals that of a model with elastic-plastic material properties everywhere. As the height of the metal layer is decreased, the FCG rate then increases. The maximum increase in FCG rate over that for the model with  $h_l / \delta_0 \rightarrow \infty$  is found to be 0.2. This value is reached for  $h_l / \delta_0 = 10$ . Beyond this value of layer height a further decrease in  $h_l / \delta_0$  has virtually no effect on the FCG rate. FCG rates are known to be connected to crack closure effects. Figure 2(b) depicts the predicted crack opening profiles,  $\Delta u_n / \delta_0$ , obtained at the minimum load in the fatigue cycle for the model with metal layer height  $h_l / \delta_0 = 10$  and the model with two ductile substrates,  $h_l / \delta_0 \rightarrow \infty$ . Data are presented for a growing fatigue crack at the end of the 29th load cycle. The corresponding normalized crack extension,  $\Delta a / \delta_0$ , is equal to 82.5 for the case  $h_l / \delta_0 = 10$  and 62.5 for the case  $h_l / \delta_0 \rightarrow \infty$ , respectively. The result demonstrates the influence of constraint on the crack closure. For  $h_l / \delta_0 \rightarrow \infty$  pronounced crack closure is present. In a situation of high mechanical constraint, however, crack closure is reduced. For  $h_l / \delta_0 = 10$  the crack is predicted to remain open at minimum load. The absence of crack closure thus contributes to the increase in the crack growth rates for cases of small values of  $h_l$  as depicted in Fig. 2(a).

The effects of constraint on FCG under variable amplitude loading were investigated. FCG simulations under consideration of a single overload were carried out. Initially, a constant amplitude load,  $\Delta G / \phi_0 = 0.15$ , was applied. In cycle  $N=25$  an overload with magnitude  $\Delta G / \phi_0 = 0.45$  was applied. Subsequently, loading is continued with the original constant amplitude. The results of predicted normalized crack extension,  $\Delta a / \delta_0$ , vs. the cycle number,  $N$  are plotted in Fig. 3. In the absence of constraint,  $h_l / \delta_0 \rightarrow \infty$ , the overload leads to the well known crack retardation effect. On the other hand, in the absence of plastic deformation,  $h_l / \delta_0 = 0$ , the overload causes an instantaneous crack advance and temporarily increased crack growth rates. For intermediate values of the height of the ductile layer,  $20 < h_l < 60$ , the crack growth behavior is found to be a combination of the two limiting cases  $h_l / \delta_0 \rightarrow \infty$  and  $h_l / \delta_0 \rightarrow 0$ . The overload results in a sequence of crack acceleration-deceleration-acceleration with the final behavior depending on the metal layer height.

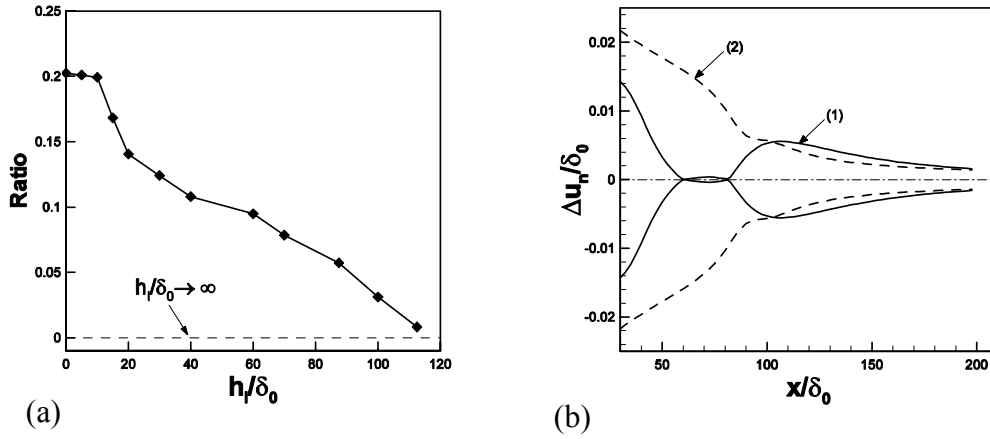


Figure 2: (a) FCG rates for various values of  $h_l / \delta_0$  compared to that for  $h_l / \delta_0 \rightarrow \infty$ ,  $\{[d(\Delta a / \delta_0) / dN]_{h_l / \delta_0} - [d(\Delta a / \delta_0) / dN]_{h_l / \delta_0 \rightarrow \infty}\} / [d(\Delta a / \delta_0) / dN]_{h_l / \delta_0 \rightarrow \infty}$ , vs. the height of the ductile layer. (b) Crack opening profiles for (1)  $h_l / \delta_0 \rightarrow \infty$  and (2)  $h_l / \delta_0 = 10$ .

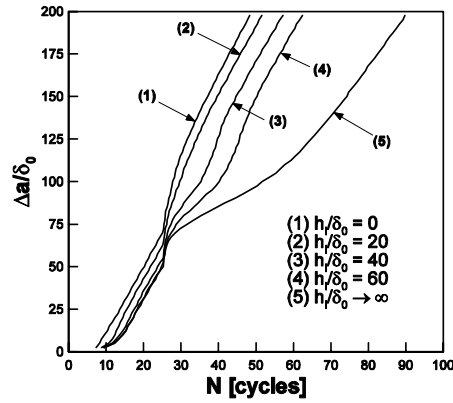


Figure 3: Normalized fatigue crack extension curves for two elastic substrates with a ductile interlayer of different sizes,  $h_l / \delta_0$ , under variable amplitude loading,  $R = 0$ .

#### 4 SIZE EFFECT

##### 4.1 Model Definition

In the second part of the paper, the effect of specimen size on the fatigue failure behavior is investigated. The notched strip model of Fig. 4 is considered. An infinite strip of height  $2h_s$  with a semi-infinite crack along the centerline of the strip is loaded by applying a cyclic uniform vertical displacement  $v(t)$  on the upper and lower edges.

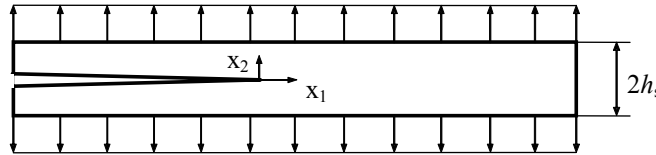


Figure 4: Schematic of a notched strip model under uniform external load.

The cyclically varying energy release rate is given by  $G(t) = 2h_s W_\infty(t)$ , where  $W_\infty(t)$  is the strain energy density at  $x_1 = \infty$  given by  $e_{11} = e_{12} = 0$ ,  $e_{22}(t) = v(t)/h_s$ . Applying the stress-strain relations for elasticity

$$\sigma_{ij} = 2\mu \left( e_{ij} + \frac{3-\kappa}{2\kappa-2} e_{kk} \delta_{ij} \right) \quad i, j, k = 1, 2 \quad (6)$$

and for plane strain,  $\kappa = 3 - 4\nu$ , we obtain

$$G(t) = 2h_s W_\infty(t) = 2h_s \frac{1}{2} \sigma_{22} e_{22} = \frac{E(1-\nu)}{2(1+\nu)(1-2\nu)} \frac{2[v(t)]^2}{h_s} \quad (7)$$

For the cyclic loading we consider  $v(t) = \Delta v(0.5 - 0.5 \cos 2\pi t)$ . A refined mesh is placed near the crack tip. The length of one square element in this uniformly meshed region is  $l = 5\delta_0$ . The height of the highly refined mesh region is  $20\delta_0$ . In the finite element model symmetry conditions are employed. Four node plain strain elements are used, and 498 CZ elements are placed along the symmetry axis from the initial crack tip to the right edge. The elastic strip is described by Young modulus,  $E = 100$  GPa, and Poisson's ratio,  $\nu = 0.34$ . For the CZ elements, the cohesive zone properties  $\phi_0 = 10$  J/m<sup>2</sup>,  $\sigma_{\max,0} = 1000$  MPa,  $\sigma_f / \sigma_{\max,0} = 0.25$  and  $\delta_\Sigma / \delta_0 = 4$  are used.

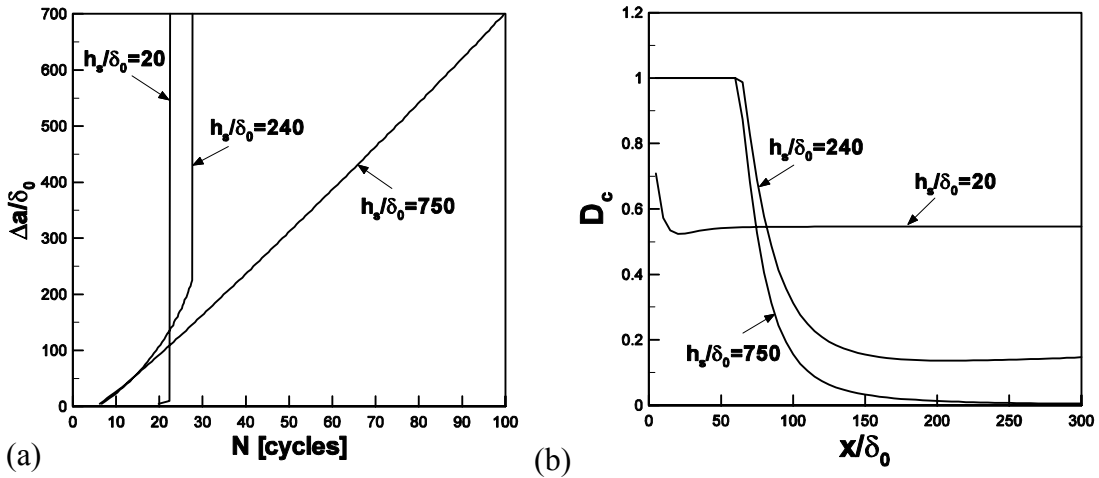


Figure 5: Predicted fatigue behaviors of a notched strip with the different normalized strip heights,  $h_s / \delta_0$ . (a) Normalized fatigue crack extension curves. (b) Distribution of fatigue damage.

#### 4.2 Results

To investigate the size effects on fatigue failure behavior models with strip heights of  $h_s / \delta_0 = 20$ , 240 and 750 were investigated under constant amplitude loading condition with  $\Delta G / \phi_0 = 0.2$  and  $R=0$ . Figure 5(a) shows the predicted normalized fatigue crack extensions for the three values of strip height. It can be seen that the fatigue failure behavior significantly depends on ratio  $h_s / \delta_0$ . In the specimen with the smallest height,  $h_s / \delta_0 = 20$ , fatigue failure is predicted to be initiation controlled. Figure 5(b) depicts the damage distribution along the ligament at time  $t=15.5$ . For  $h_s / \delta_0 = 20$  damage occurs essentially through a process of uniform cyclic debonding along the ligament in front of the initial crack tip. At  $t=15.5$  damage has not yet reached  $D_c=1$  and the crack

has not extended. On the other hand, for the specimen with the largest height,  $h_s / \delta_0 = 750$ , the fatigue failure behavior displays a behavior characterized by crack growth initiation and subsequent growth. The behavior of the specimen with intermediate height,  $h_s / \delta_0 = 240$  initially follows that of  $h_s / \delta_0 = 750$ , however, the crack growth rate is larger than for  $h_s / \delta_0 = 750$  and an abrupt transition to a uniform debonding occurs later. For the largest specimen,  $h_s / \delta_0 = 750$ , a damage distribution typical of a cracked structure is present. Damage has reached a distinct maximum at the current crack tip,  $D_c = 1$ . For locations further away from the crack tip, damage has not yet accumulated. For the intermediate size specimen  $D_c = 1$  at the current crack tip. Here, however, damage has also accumulated even far from the crack tip. The present finding on the size effect in damage distribution is in agreement with results of recent investigations on the size effects of strength [13]. There, it was shown that in small specimens a constant value of stresses is present in front of the crack tip while for larger specimens a crack tip type field dominates.

## 5 CONCLUSION

The present paper describes results on simulations of fatigue failure conducted by use of an irreversible cohesive zone model. Constraint effects in multilayer structures are demonstrated to alter fatigue crack growth rates through changes in the crack closure behavior. The cohesive zone model approach is useful in this context as the effects of constraint are a direct outcome of the model and no a-priori specification of constraint factors are required.

It is demonstrated that specimen size can alter the characteristics of the fatigue failure behavior. When the sample size is sufficiently small, the stress distribution is constrained by the specimen boundary. The crack type stress distribution found in large specimens cannot develop, the stress concentration disappears and the damage distribution in the specimen becomes uniform. The cohesive zone model approach is also useful here since it captures both the S-N type behavior of the small specimens as well as the Paris type behavior found at large structural sizes.

## 6 ACKNOWLEDGEMENTS

Funding for this work by was provided by the Air Force Office of Scientific Research under contract F49620-03-1-0152.

## 7 REFERENCES

- [1] Varias, A.G., Suo, Z., Shin, C.F., *J. Mech. Phys. Solids* 39, 963-986, (1991)
- [2] Evans, A.G., Hutchinson, J.W., *Acta Metall. Mater.* 43, 2507-2530, (1995)
- [3] Dauskardt, R.H., Lane, M., Ma, Q., Krishna, N., *Eng. Fract. Mech.* 61, 141-162, (1998)
- [4] Lane, M., Dauskardt, R.H., Vainchtein, A., Gao, H., *J. Mater. Res.* 15, 2758-2769, (2000)
- [5] Ji, B., Gao, H., *Mat. Sci. Eng. A366*, 96-103, (2004)
- [6] Gao, H., Ji, B., Jäger, I.L., Arzt, E., Fratzl, P., *Proc. Natl. Acad. Sci.*, 100, 5597-5600, (2003)
- [7] Tvergaard, V., Hutchinson, J.W., *Philos. Mag.* A70, 641-656, (1994)
- [8] Tvergaard, V., Hutchinson, J.W., *J. Mech. Phys. Solids* 44, 789-800, (1996)
- [9] Tvergaard, V., Hutchinson, J.W., *J. Mech. Phys. Solids* 40, 1377-1397, (1992)
- [10] Lin, G., Kim, Y.J., Cornec, A., Schwalbe, K.H., *Comp. Mater. Sci.* 9, 36-47, (1997)
- [11] McNaney, J.M., Cannon, R.M., Ritchie, R.O., *Acta Mater.* 12, 4713-4728, (1996)
- [12] Kruzic, J.J., McNaney, J.M., Cannon, R.M., Ritchie, R.O., *Mech. Mater.* 36, 57-72, (2004)
- [13] Gao, H., Ji, B., *Eng. Fract. Mech.* 70, 1777-1791, (2003)
- [14] Roe, K.L., Siegmund, T., *Eng. Fract. Mech.* 70, 209-232, (2003)
- [15] Ma, F., Sutton, M.A., Deng, X., *J. Mech. Phys. Solids* 49, 2921-2953, (2001)
- [16] Gao, X., Shih, C.F., *Eng. Fract. Mech.* 60, 407-420, (1998)
- [17] Roychowdhury, S., Robert, H., Dodds, Jr., *Eng. Fract. Mech.* 70, 2363-2383, (2003)